LA-UR-80-3295

CONF-8006139--1

TITLE: DETECTION OF A THIN SHEET MAGNETIC ANOMALY BY SQUID-GRADIOMETER SYSTEMS: POSSIBILITY OF HYDROFRACTURE AZIMUTH DETERMINATION.

MASTER

AUTHOR(S): W. C. Overton, Jr.

SUBMITTED TO: PROCEEDINGS OF THE SQUID APPLICATIONS TO GEOPHYSICS WORKSHOP held 2-4 June, 1980 at Los Alamos, H. Weinstock and W. C. Overton, Jr., editors, Society of Exploration Geophysicists, Tulsa, Oklahoma, 1980.

DISCLAIMER

This book was prepared as an account of work sponsored by an agency of the United States Government. Neither the United States Government nor any agency thereof, nor any of their employees, makes any warranty, express or implied, or assumes any legal liability or responsibility for the accuracy, completeness, or usefulness of any information, apparatus, product, or process disclosed, or represents that its use would not infringe privately owned rights. Reference herein to any specific commercial product, process, or service by trade name, trademark, manufacturer, or otherwise, does not necessarily constitute or imply its endorsement, recommendation, or favoring by the United States Government or any agency thereof. The views and opinions of authors expressed herein do not necessarily state or reflect those of the United States Government or any agency thereof.

University of California

By acceptance of this article, the publisher recognizes that the U.S. Government retains a nonexclusive, royalty-free license to publish or reproduce the published form of this contribution, or to allow others to do so, for U.S. Government purposes.

The Los Alamos Scientific Laboratory requests that the publisher identify this article as work performed under the auspices of the U.S. Department of Energy.

LOS ALAMOS SCIENTIFIC LABORATORY
Post Office Box 1663 Los Alamos, New Mexico 87545
An Affirmative Action/Equal Opportunity Employer

DISTRIBUTION OF THIS DOCUMENT IS UNLIMITED

Form No. 836 R3
St. No. 2629
12/78

UNITED STATES
DEPARTMENT OF ENERGY
CONTRACT W-7405-ENG. 36

DISCLAIMER

This report was prepared as an account of work sponsored by an agency of the United States Government. Neither the United States Government nor any agency Thereof, nor any of their employees, makes any warranty, express or implied, or assumes any legal liability or responsibility for the accuracy, completeness, or usefulness of any information, apparatus, product, or process disclosed, or represents that its use would not infringe privately owned rights. Reference herein to any specific commercial product, process, or service by trade name, trademark, manufacturer, or otherwise does not necessarily constitute or imply its endorsement, recommendation, or favoring by the United States Government or any agency thereof. The views and opinions of authors expressed herein do not necessarily state or reflect those of the United States Government or any agency thereof.

DISCLAIMER

Portions of this document may be illegible in electronic image products. Images are produced from the best available original document.

This preliminary version has been refereed and edited.

DETECTION OF A THIN SHEET MAGNETIC ANOMALY BY SQUID-GRADIOMETER SYSTEMS: POSSIBILITY OF HYDROFRACTURE AZIMUTH DETERMINATION*

W. C. Overton, Jr. #

ABSTRACT

We have carried out a study of the signal physics of magnetic anomaly detection by superconducting gradiometer and magnetometer loop systems with SQUID sensors for possible application to the LASL geothermal energy program. In particular, the crack produced by hydrofracture of a deep HDR geothermal borehole would be filled with a magnetic material such as ferrofluid. When polarized by the earth's field, this material would produce a localized crack magnetic anomaly which is characteristic of the azimuth of the vertical crack with respect to magnetic north. Signatures of the anomaly would be determined by taking rotation data before and after filling the crack with magnetic material. We have found a mathematical description for these signatures. To test the theory and the feasibility of the idea, we simulated the deep borehole vertical cracks by using ing panels to define sheets 1.5 mm thick, 1.2 m wide, and 2.5 m high. When filled with ferrofluid of suitable magnetic permeability, the local anomaly develops. Signatures were measured with a horizontal axial gradiometer rotated about a vertical axis. We find good agreement between theory and experiment for azimuths in the east and west quadrants, but only fair agreement in the north and south quadrants.

I. INTRODUCTION.

In the past twelve years, both rf and dc SQUIDs have evolved into reliable instruments for measuring small changes in magnetic fields. When a superconducting magnetometer pickup loop is used in conjunction with a typical commercial rf SQUID, one can detect by this system changes as small as 10^{-10} G with a 1.0 Hz instrumental bandwidth (See reviews by Giffard, et al, 1972; Clarke, 1973). When two identical spatially-separated loops are connected in opposition, the current coupled to the SQUID sensor is proportional to the spatial derivative of the external magnetic field in the direction of the axis common to the two loops. In this so-called gradiometer mode, magnetic noise interference is significantly reduced, and system sensitivities as high as 10^{-8} to 10^{-9} G per cm per $(\text{Hz})^{1/2}$ are possible. Meanwhile, specially designed dc SQUIDs (Clarke, et al, 1976) and rf SQUIDs (Long, et al, 1980) have sensitivities one to two orders of magnitude better than those mentioned above.

Such developments allow many new types of sensitive measurements that were not possible by earlier methods. A few examples of SQUID-gradiometer or magnetometer uses are: diagnostic tools in medicine such as the magnetocardiogram and magnetoencephalogram; in biology the observation of nerve current impulses; in geophysics, SQUID-magnetotelluric exploration; and numerous applications in physics.

We consider in this report an application in geophysics which should make possible the determination of the azimuth of a thin hydrofracture crack near the bottom of a deep borehole after it has been flooded with ferrofluid. This capability may prove to be of value to the hot-dry-rock (HDR) geothermal energy program of the Los Alamos Scientific Laboratory.

In principle, the HDR geothermal energy program involves: (1) the drilling of a borehole to a depth of 2,500 m (8,000 ft) or more into an HDR zone; (2) the application of high pressures to borehole fluids to produce hydraulic fracturing of the rock zones near the borehole bottom; (3) location of the splits, cracks, or fissures produced by this hydrofracturing; and (4) drilling a second borehole some 100 to 300 m from the first so as to intersect the fractured zones (See Albright and Newton, 1980). In practical use, water pumped down one borehole would flow through these cracks to the second borehole, become heated by the HDR's in the process, and emerge as steam to run an electric power plant.

Because of the very great expense of deep borehole drilling, significant economies will result if the approximate azimuth of the hydrofracture crack system is known prior to drilling the second borehole. A requirement on the accuracy of this azimuth determination has been suggested as ± 15° (Tester and Spence, 1980).

Our application mentioned above involves the use of a SQUID-gradiometer and/or magnetometer system located in a cryogenic environment which, in turn, is to be housed in a logging tool. This system would then be positioned in the borehole adjacent to the hydrofracture crack. We impose a further requirement that the horizontal-axial or hori-

* Work performed under the auspices of U.S.D.O.E.

Los Alamos Scientific Laboratory, P.O. Box 1663, Los Alamos, NM 87544.

zontal planar gradiometer or horizontal axis magnetometer must be rotated about a vertical axis in order to obtain the magnetic anomaly data due to the hydrofracture crack. The magnetic signal picked up will be recorded in the form of amplitude of the field (in G) or amplitude of the field derivative (in G/cm) as a function of the angular position of the axis of the magnetometer or gradiometer with respect to magnetic north. We show below that it is these angular dependences that characterize the azimuth of the hydrofracture crack after it has been filled with ferromagnetic fluid. In other words, the rotation signal exhibits a signature which is characteristic of the azimuth of the crack.

When this concept was first examined by the author (Overton, 1976) the magnetic materials then considered for flooding into the hydrofracture crack were various paramagnetics and colloidal size iron or ferrite particles in suspension. The analysis showed that the various paramagnetic substances in solution would exhibit such a small magnetic moment at high temperatures as to be barely observable as a crack anomaly by a SQUID-gradiometer system in the borehole. On the other hand, colloidal-sized iron or ferrite particles seemed to offer a possible solution to the problem because the magnetic moment per particle remained large even at temperatures as large as 800 K. The Curie point of the iron particles is 1,040 K. Unfortunately, a colloidal suspension of such materials would be very expensive.

In 1978, we focused attention on magnetite ferrofluid as a better alternative than the colloidal suspensions of solid iron or ferrite particles mentioned above. While this ferrofluid could be obtained in small commercial quantities for about $800 per liter, there was a process (Reimers and Khallafalla, 1974) for low cost production of large quantities. Following this formula, we produced in the laboratory some 140 liters for only about $50 per liter with the promise that this could be reduced to less than $5 per liter in local large scale production. Since only the bottom 100 m or so of a borehole needs to be filled with ferromagnetic fluid to flood the material in the HDR hydrofracture cracks, the total amount of fluid required would be fairly small. Thus, this manufacturing cost reduction is a significant factor in estimating the overall feasibility of this project.

We discuss in Section II the polarization of a magnetic anomaly by the earth's field. The quantity of interest is the magnetic moment that will result when a superparamagnetic material such as ferrofluid is placed in this weak polarizing field.

In Section III we study the more general problem of how fields at any point are modified by the presence of an arbitrary deep distribution of magnetic material which has become polarized by the earth's field.

In Section IV we show how these same equations can be adapted to describe the response of a rotating superconducting gradiometer or magnetometer to an anomaly caused by an arbitrary distribution of magnetic material. The measuring system can be either in the borehole near a localized anomaly of small volume or a great distance away from a large source.

We discuss in Section V the experimental setup for our SQUID gradiometer system and its non magnetic rotating platform, the ferrofluid-filled thin sheet which simulates the hydrofracture crack, and other details of the experiment.

We compare in Section VI the experimental gradiometer rotation data with the theoretical predictions of Section IV. We present the results of cross-correlation calculations and least squares adjustments of these two sets of data and are able to show that the ± 15° criterion on the accuracy of crack azimuth determination is satisfied for the east and west quadrants. Further study and measurements will be required to determine if the criterion can be satisfied for azimuths in the north and south quadrants.

In Section VII we give a summary of the work and discuss future potentialities.

II. POLARIZATION BY THE EARTH'S FIELD.

The earth's field horizontal component H_h and vertical component H_v can be estimated at any set of geographical coordinates on the surface by the use of well-known formulas (Segiura and Heppner, 1972) based on the assumption of a dipole located at the earth's center. These fairly accurate estimates take the forms:

$$H_h = H_e(a/r_a)^3 \sin \theta_e \ ,$$

$$H_r = 2H_e(a/r_a)^3 \cos \theta_e \ ,$$

$$H_e = 0.3035 \ ,$$

$$a = 6.371 \times 10^8 \text{ cm } (6{,}371.2 \text{ km}) \ , \qquad (1)$$

where a is the reference radius for a spherical earth and r_a is the radius to the point in question. We usually assume $r_a = a$, especially for points near the surface. The angle θ_e is defined as the geomagnetic colatitude according to

$$\cos \theta_e = \cos u \cos u_o + \sin u \sin u_o \cos(w - w_o) \ , \qquad (2)$$

where u is the geographic colatitude, $u_o = 11.44°$ is the geographic colatitude of the magnetic north pole, and $w_o = 290.24°$ is the east longitude of the north pole.

As an example, we consider a location in the

Jemez Mountains of New Mexico near the Fenton Hill HDR Geothermal Energy Site of the Los Alamos Scientific Laboratory. ere, the geographical coordinates are approximately 35° 55'N, 106° 30'W, which corresponds to colatitude 54.083° and east longitude 253.5°. Substituting in Eq.(2), we find for the estimated local field values,

$$H_h = 0.2199 \text{ Oe} ; \quad B_h = 0.2199 \text{ G} ;$$
$$H_v = 0.4356 \text{ Oe} ; \quad B_v = 0.4356 \text{ G} ;$$
$$H_o = 0.4880 \text{ Oe} ; \quad B_o = 0.4880 \text{ G} ; \qquad (3)$$
$$\psi = \tan^{-1} H_v/H_h ,$$

where H_o and B_o are the total field and induction, respectively, in emu units.

In the remainder of this paper we shall employ SI units in which $\underset{\sim}{B} = \mu_m \underset{\sim}{H} = k_m \mu_o \underset{\sim}{H}$, μ_m is the magnetic permeability of a medium with label m, μ_o ($= 4\pi \times 10^{-7}$ H/m) is the free-space permeability, and k_m is the dimensionless permeability.

The vector induction $\underset{\sim}{B}$ of the earth's field polarizes any isolated distribution of magnetic material having a magnetic permeability $k_{in}\,\mu_o$ which is embedded in external material of permeability $k_{ex}\,\mu_o$ where $k_{in} \neq k_{ex}$. When $k_{in}/k_{ex} > 1$, then the polarization is termed paramagnetic and when $k_{in}/k_{ex} < 1$, the body is diamagnetic. Both paramagnetic (ferrous-like) deposits and diamagnetic (oil and coal) deposits give rise to magnetic anomalies. The existence of such anomalies can sometimes be discerned by magnetic surveys. When SQUID gradiometer and magnetometer systems are used for such surveys, the probability of detecting these anomalies should be enhanced.

The shape of the boundary surface between the magnetic body and its embedding medium determines the strength and direction of the induced magnetization inside the body. This comes about through the formal boundary conditions,

$$\underset{\sim}{B}_{ex} \cdot \underset{\sim}{n} = \underset{\sim}{B}_{in} \cdot \underset{\sim}{n} \text{ ; or}$$

$$k_{ex}\,\mu_o \underset{\sim}{H}_{ex} \cdot \underset{\sim}{n} = k_{in}\,\mu_o \underset{\sim}{H}_{in} \cdot \underset{\sim}{n} ;$$

$$\underset{\sim}{H}_{ex} \times \underset{\sim}{n} - \underset{\sim}{H}_{in} \times \underset{\sim}{n} = \underset{\sim}{K} , \qquad (4)$$

where $\underset{\sim}{n}$ is the surface normal vector, $\underset{\sim}{K}$ is the surface current density, and $\times$ denotes vector product. In the present case of magnetostatic polarization, $K = 0$.

We show in Fig. 1 a vertical hydrofracture crack extending to $+\infty$ in the radial direction at angle ϕ (with respect to the x-axis or magnetic north), to $+\infty$ in the + z-direction (above plane of paper) and to $-\infty$ in the minus z-direction (below plane of paper) We assume the magnetic induction due to the earth's field is of the vector form,

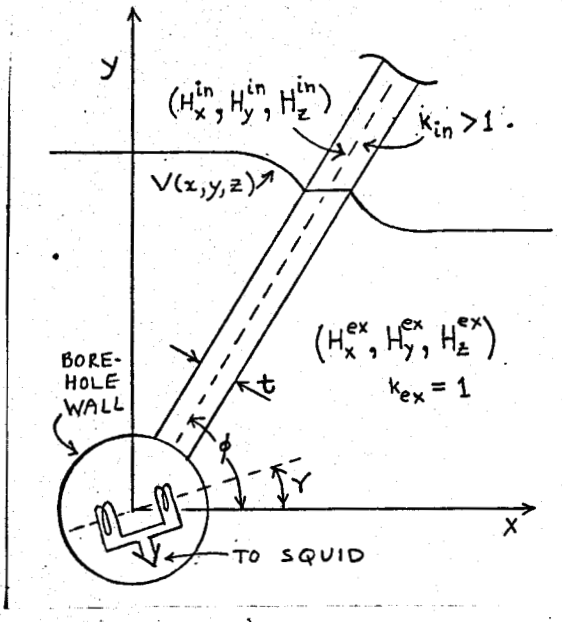

Fig. 1. Schematic showing vertical hydrofracture crack extending outward from borehole into formation rocks at an angle ϕ with respect to x-axis (magnetic north). Crack thickness t as shown here is exagerated. Crack is assumed filled with ferrofluid of magnetic permeability $k_{in} > 1$. Field components at a point (x,y,z) inside crack are H_x^{in}, etc. Outside, at any point (x,y,z) where $k_{ex} = 1$, the field components are H_x^{ex}, etc. Typical streamlines of the scalar magnetic potential function V(x,y,z) are shown bending into the magnetic material at close range but asymptotically at large distances, they become parallel to the earth's field. A superconducting gradiometer pickup loop system is shown schematically at the center of the borehole.

$$\underset{\sim}{B} = \underset{\sim}{i} B_x + \underset{\sim}{j} B_y + \underset{\sim}{k} B_z , \qquad (5)$$

where $(\underset{\sim}{i}, \underset{\sim}{j}, \underset{\sim}{k})$ are unit vectors for the coordinate system of Fig. 1. We consider a unit normal vector

$$\underset{\sim}{n} = \underset{\sim}{i} \sin\phi - \underset{\sim}{j} \cos\phi , \qquad (6)$$

as shown extending from a point (x_b, y_b, z_b) on the right side boundary plane of the crack. Applying the formal boundary conditions (4), we find at any such point (x_b, y_b, z_b) on this plane,

$$\cos\phi\, H_x^{ex} + \sin\phi\, H_y^{ex} = \cos\phi\, H_x^{in} + \sin\phi\, H_y^{in} , \qquad (7)$$

$$H_z^{ex} = H_z^{in} , \qquad (8)$$

$$\sin\phi\, H_x^{ex} - \cos\phi\, H_y^{ex} = k_{in}(\sin\phi\, H_x^{in} - \cos\phi\, H_y^{in}) , \qquad (9)$$

where we assume $k_{ex} = 1$. The boundary conditions on the narrow edge boundary (length = thickness t) can be determined by the same process. The results can be expressed by modification of (7)-(9) as follows: In (7), interchange cos ϕ with sin ϕ and change

the plus sign to a minus sign. There is no change in (8). In (9) interchange cos ϕ with sin ϕ and change the minus sign to plus sign. Since the crack thickness t is very small, we shall not need these latter boundary conditions in our later dipole type of analysis. However, they would be needed if we should choose to evaluate the scalar magnetic potential function V(x,y,z).

Combining (7) and (9), we evaluate the components H_x^{in}, H_y^{in} inside the crack in terms of the external components evaluated at the common point on the boundary. We obtain

$$kH_x^{in} = (k\cos^2\phi + \sin^2\phi)H_x^{ex} + (k-1)\sin\phi\cos\phi\, H_y^{ex},$$

$$kH_y^{in} = (k-1)\sin\phi\cos\phi\, H_x^{ex} + (k\sin^2\phi + \cos^2\phi)H_y^{ex}, \tag{10}$$

where now k denotes k_{in} and $k_{ex} = 1$.

It is of interest to calculate the density of magnetostatic energy inside the crack. This is given by $(1/2)\underset{\sim}{B}\cdot\underset{\sim}{H}$ (units are J/m^3) and can be expressed in the form,

$$W_{in} = (k\mu_o/2)\left[(H_x^{in})^2 + (H_y^{in})^2 + (H_z^{in})^2\right]. \tag{11}$$

Using the results given by (10), we obtain

$$W_{in} = (\mu_o/2k)\left[k^2(\cos\phi\, H_x^{ex} + \sin\phi\, H_y^{ex})^2 + (\sin\phi\, H_x^{ex} - \cos\phi\, H_y^{ex})^2\right] + k\mu_o(H_z^{ex})^2/2 , \tag{12}$$

in which the first parentheses within the square brackets is the tangential component, i.e., component parallel to the sidesurface at the boundary. The second set of parentheses is the normal component of external $\underset{\sim}{H}$ at the boundary. Since the z-components cancel between (11) and (12), it is convenient to define the quantities h_{in} and h_{ex} according to

$$h_{in}^2 = (H_x^{in})^2 + (H_y^{in})^2 \quad ; \quad h_{ex}^2 = (H_x^{ex})^2 + (H_y^{ex})^2 . \tag{13}$$

Thus, the directions in the x-y plane of Fig. 1 of the vectors $\underset{\sim}{h}_{in}$ and $\underset{\sim}{h}_{ex}$ can be defined in terms of the angles p and q, respectively, according to

$$H_x^{in} = h_{in}\cos p \quad ; \quad H_y^{in} = h_{in}\sin p \quad ;$$

$$H_x^{ex} = h_{ex}\cos q \quad ; \quad H_y^{ex} = h_{ex}\sin q \quad , \tag{14}$$

where these angles are measured with respect to the x-axis (magnetic north) of Fig. 1. Accordingly, using Eqs. (12)-(14), we obtain the relation

$$h_{ex}^2 = k^2 h_{in}^2 / \left[k^2\cos^2(\phi-q) + \sin^2(\phi-q)\right] . \tag{15}$$

Some properties of this important relation can be deduced directly. For example, when $\phi = 0$, the crack of Fig. 1 is parallel to the earth's field and the tangential components of $\underset{\sim}{H}$ must be continuous in order to satisfy (4), i.e., $\underset{\sim}{h}_{ex}$ must equal $\underset{\sim}{h}_{in}$. Similarly, when $\phi = 90°$, the normal component of B must be continuous, i.e., $h_{ex} = kh_{in}$. Again, the boundary conditions require $p = 0$ and $q = 0$.

It is important to establish the relationship between p, q, and ϕ for angles ϕ other than 90° and 0° (. This can be done by considering small values of the angles p and q for small deviations of ϕ from 90° or 0°. For the case near 90° let $\phi = \pi/2 - d\phi$ and assume p and q take on small values to be determined. Substituting in Eq. (10), expanding the sine and cosine terms, and using (14), we obtain

$$k(h_{in} + dh_{in})(1 - p^2/2 + \ldots) = (h_{ex} + dh_{ex}) \times \left[1 + kd\phi(d\phi + q) - d\phi^2 - (q^2 + 2qd\phi)/2 + \mathcal{O}(4)\right]$$

terms , (16)

$$k(h_{in} + dh_{in})(p - p^3/6 + \ldots) = (h_{ex} + dh_{ex}) \times \left[k(d\phi + q) - d\phi + \mathcal{O}(3)\right] \quad . \tag{17}$$

Comparing zero order terms in (16), we note that $kh_{in} = h_{ex}$, just as at $\phi = 90°$. From (17), we find both $kh_{in}p = h_{ex}(kd\phi + kq - d\phi)$ in first order and $kdh_{in}p = dh_{ex}(kd\phi + kq - d\phi)$ in 2nd order. This relationship from (17) requires either $p = 0$ or that $kdh_{in} = dh_{ex}$. To test the latter, we can differentiate the energy relationship (15), letting $\phi = 90° - d\phi$ and $dq = q$. This analysis leads to a second order difference relationship

$$(kdh_{in} - dh_{ex}) = h_{ex}(k^2-1)(q + d\phi)^2 .$$

Thus, since $kdh_{in} \neq dh_{ex}$, we conclude p must equal zero. As a further check, we let $p = 0$ in (16) and solve the quadratic due to the second order terms. This leads to the result already obtained from the analysis of (15).

The above proofs that $p = 0$ for various ϕ angles in the vicinity of $\phi = 90°$ (and near $\phi = 0°$, by similar procedures) provides only necessary conditions that $p = 0$, but not sufficient conditions for all values of ϕ. A general proof is beyond the scope of the present paper. However, we believe the above result is general and shall now assume $p = 0$ for all other angles ϕ. Referring to Eq. (14), this is equivalent to the proof that $H_y^{in} = 0$. Thus, using $H_y^{in} = 0$ in (10), leads directly to the following relationship between ϕ and q, namely,

$$k\tan\phi = \tan(\phi - q) \quad . \tag{18}$$

As a result of these findings, we reach the following conclusions: When the crack is oriented to arbitrary ϕ values, the three-dimensional streamlines of the scalar magnetic potential function $V_{ex}(x,y,z)$ will be curved, as indicated schematically in Fig. 1. Thus, since $H_x = -\partial V/\partial x$, $H_y = -\partial V/\partial y$, the angle $q = \tan^{-1}(H_y/H_x)$ will be determined by the

relation (18) at any boundary point on the sidewall surface of the ferrofluid-filled sheet. The projection of typical streamlines on the - plane is shown schematically in Fig. 1. However, inside the sheet, where we have found p = 0, the streamlines of $V_{in}(x,y,z)$ are straight lines so that the projection on the x-y plane is a horizontal line, i.e., with no y-component, as in Fig. 1.

It is of interest to examine the angle q at the surface obtained by projecting the vector $\underset{\sim}{H}^{ex}$ onto an x-y plane. We show in Table 1 some solutions of Eq. (16) for various azimuth values in the first quadrant of Fig. 1. and for various values of the magnetic permeability $k = k_{in}$. The range of k_{in} shown is typical for ferrofluids we might expect to use in a hydrofractured borehole.

Table 1.

The angle q (tabulated in degrees) of the vector h_{ex}, as defined by Eq. (14), that satisfies the relation (18) for various azimuth angles, ϕ s, and values of the magnetic permeability, k_{in}.

k_{in} \ ϕ	15°	30°	45°	60°	75°
1.10	-1.42	-2.42	-2.73	-2.31	-1.31
1.15	-2.13	-3.58	-3.99	-3.34	-1.88
1.20	-2.83	-4.72	-5.19	-4.31	-2.41
1.25	-3.52	-5.82	-6.34	-5.21	-2.90
1.30	-4.21	-6.89	-7.43	-6.05	-3.35
1.40	-5.56	-8.95	-9.46	-7.59	-4.17
1.60	-8.21	-12.73	-12.99	-10.16	-5.49
1.80	-10.78	-16.10	-15.95	-12.22	-6.53
2.00	-13.19	-19.11	-18.44	-13.90	-7.37

The q values of Table 1. are all negative for the vector h_{ex} extending from a point on the surface of the right sheet boundary of Fig. 1. The corresponding values for a vector on hhe left boundary are the same numerically as those in Table 1. but the signs are all positive. It is easy to see from Fig. 1. that if the crack azimuth is between 90° and 180°, the angles for the right boundary would be positive while those for the left boundary would be negative. Similarly, for the third and fourth quadrants of Fig. 1., we can find the correct angle q by simply using the appropriate sign changes in Table 1.

It is useful to express the result (10) in terms of the magnetic susceptibility $\chi_{in} = k_{in} - 1$ of the ferrofluid. Since we have found $H_y^{in} = 0$, we have, from the second equation of (10),

$$H_y^{ex}(1 + \chi_{in}\sin^2\phi) = -\sin\phi\cos\phi\, H_x^{ex} ,$$

which leads to,

$$H_y^{ex}/H_x^{ex} = \tan q = -\chi_{in}\sin\phi\cos\phi/(1 + \chi_{in}\sin^2\phi), \quad (19)$$

This equation is just an equivalent form of (18) and gives the same results as in Table 1. However, when we use (19) to eliminate H_y^{ex} in (18), we obtain

$$(1 + \chi_{in})H_x^{in} = H_x^{ex}\left[(1 + \chi_{in}\cos^2\phi) - \chi_{in}^2\sin^2\phi\cos^2\phi/(1 + \chi_{in}\sin^2\phi)\right] ,$$

$$= H_x^{ex}(1 + \chi_{in})/(1 + \chi_{in}\sin^2\phi) . \quad (20)$$

This relation shows that when the magnetic susceptibility $\chi_{in} \to 0$, $H_x^{in} = H_x^{ex}$, as it should. However, since $H_x^{ex} = H_o\sin\psi\cos q$, we find,

$$H_x^{in} = H_o\sin\psi\cos q/(1 + \chi_{in}\sin^2\phi)$$

$$H_y^{ex} = -\chi_{in}H_o\sin\psi\cos q\sin\phi\cos\phi/(1+\chi_{in}\sin^2\phi). \quad (21)$$

Using these results we can now calculate the magnetic moment per unit volume for volume elements of the sheet.

The Magnetization

The magnetization, or magnetic moment per unit volume, of a volume element dxdydz inside the ferrofluid material of the sheet, is determined by the standard relationship,

$$\underset{\sim}{m} = \underset{\sim}{B}^{in}/\mu_o - \underset{\sim}{H}^{in} . \quad (22)$$

The magnetic induction $\underset{\sim}{B}^{in} = k\,\mu_o\underset{\sim}{H}^{in}$ can be expressed in terms of Eqs. (8), and (20) or (21). We find

$$\underset{\sim}{m} = \left[\underset{\sim}{i}\,k_{in}H_o\sin\psi\cos q/(1 + \chi_{in}\sin^2\phi) + \underset{\sim}{k}\,k_{in}H_o\cos\psi\right] - \underset{\sim}{H}^{in} , \quad (23)$$

where q is defined by (19). Letting $(k_{in}-1)H_o = m_o = \chi_{in}H_o$ and $\sin\psi' = \sin\psi\cos q/(1 + \chi_{in}\sin^2\phi)$, we have $m_x = m_o\sin\psi'$, $m_z = m_o\cos\psi$.

With these results, we can now calculate the fields at any position outside the ferrofluid filled sheet due to the distribution of dipole moments, each with strength $\underset{\sim}{m}$ dxdydz.

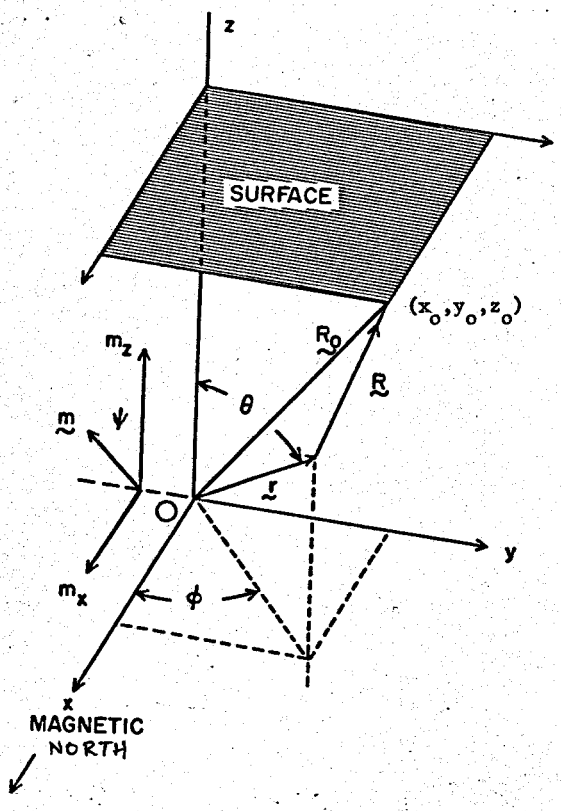

Figure 1. Coordinate system for calculating the magnetic field at any point (x_o,y_o,z_o), such as the particular point shown above on the surface, due to a single dipole of magnetic moment $m\,dx\,dy\,dz$ at the tip of vector r. In Eq. (23) we see that $m_y = 0$, $m_z = m_o\cos\psi$, but $m_x = m_o\sin\psi'$, where $\sin\psi'$, defined after Eq. (23), is slightly different from $\sin\psi$. The vector $\underset{\sim}{R}$ extends from this elemen- dipole to the point at which we wish to calculate the field. The vector $\underset{\sim}{R}_o$ from the origin of coordinates to this point. The point in question could be inside a borehole near the axis of z rather than on the surface as shown. If we choose the + x direc- as magnetic south, rather than magnetic north, m_x, H_x, and H_y will be reversed but m_z, H_z will remain unchanged.

III. FIELDS DUE TO A DISTRIBUTION OF DIPOLE MOMENTS

A. The Basic Equations.

The magnetic field H and magnetic induction B can be calculated, in principle, at any point outside of any arbitrary distribution of magnetic dipoles. In the present case, the distribution of the elementary magnetic moments of all of the volume elements inside of the thin magnetic sheet is assumed to be uniform with all elements having the same magnetization.

Let $m_o dx\,dy\,dz$ be the magnitude of the magnetic moment of the volume element dx dy dz at the point (x,y,z) in the sheet of Fig. 1, where m_o is the moment per unit volume. The vector moment, Eq. (23), is

$$\underset{\sim}{m} = \underset{\sim}{i}\, m_x + \underset{\sim}{k}\, m_z; \quad m_y = 0,$$
$$m_x = m_o\sin\psi' \; ; \; m_z = m_o\cos\psi \; . \qquad (24)$$

If $\underset{\sim}{m}$ is the moment at the tip of vector $\underset{\sim}{r}$, the contribution to the field $d\underset{\sim}{H}$ at $\underset{\sim}{R}$ can be expressed, according to dipole theory, in terms of parallel and perpendicular components $\underset{\sim}{H}_p$ and $\underset{\sim}{H}_+$, respectively, by

$$\underset{\sim}{H}_p = 2\,\underset{\sim}{R}\,(\underset{\sim}{R}\cdot\underset{\sim}{m})dx\,dy\,dz/R^5, \qquad (25)$$

$$\underset{\sim}{H}_+ = (\underset{\sim}{R}\times\underset{\sim}{R}\times\underset{\sim}{m})dx\,dy\,dz/R^5, \qquad (26)$$

$$R^2 = (x_o-x)^2 + (y_o-y)^2 + (z_o-z)^2 \; , \qquad (27)$$

$$r^2 = x^2 + y^2 + z^2 \; , \qquad (28)$$

$$R_o^2 = x_o^2 + y_o^2 + z_o^2 \; . \qquad (29)$$

The parallel component is in the direction parallel to vector $\underset{\sim}{R}$ while the perpendicular component is in the plane common to magnetic moment vector $\underset{\sim}{m}$ and vector $\underset{\sim}{R}$ but perpendicular to $\underset{\sim}{R}$.

Expanding the dot product expression in (25), the cross product expression in (26), and letting $m_o dx\,dy\,dz = dm$, we obtain the expressions,

$$dH_{px} = 2\,dm\,[(x_o-x)^2\sin\psi' + (x_o-x)(z_o-z)\cos\psi]/R^5, \qquad (30)$$

$$dH_{py} = 2\,dm\,[(x_o-x)(y_o-y)\sin\psi' + (y_o-y)(z_o-z)\cos\psi]/R^5 \; , \qquad (31)$$

$$dH_{pz} = 2\,dm\,[(x_o-x)(z_o-z)\sin\psi' + (z_o-z)^2\cos\psi]/R^5 \; , \qquad (32)$$

$$dH_{+x} = dm\,[-(y_o-y)^2\sin\psi' - (z_o-z)^2\sin\psi' + (x_o-x)(z_o-z)\cos\psi]/R^5 \; , \qquad (33)$$

$$dH_{+y} = dm\,[(x_o-x)(y_o-y)\sin\psi' + (y_o-y)(z_o-z)\cos\psi]/R^5 \; , \qquad (34)$$

$$dH_{+z} = dm\,[(x_o-x)(z_o-z)\sin\psi' - (x_o-x)^2\cos\psi - (y_o-y)^2\cos\psi]/R^5 \; . \qquad (35)$$

The field component at any point (x_o,y_o,z_o) external to the sheet distribution can be calculated by combining either (30) and (33), (31) and (34), or (29) and (35), and performing the integration over the coordinates (x,y,z) within the sheet. For example, for the x-component, we would have

$$H_x(x_o,y_o,z_o) = \int (dH_{px} + dH_{tx})dxdydz \quad . \qquad (36)$$

In performing the steps indicated by (36), we find that the numerator of the integrand of (36) can be reexpressed in the form

$$3(x - x_o)^2 \sin\psi' + 2(x - x_o)(z - z_o)\cos\psi$$
$$- [(x - x_o)^2 + (y - y_o)^2 + (z - z_o)^2]\sin\psi'. \qquad (37)$$

Accordingly, it is necessary to perform three integrations in order to evaluate H_x, e.g.,

$$H_{x1} = 3m_o \sin\psi' \iiint dxdydz\,(x-x_o)^2/R^5 \quad , \qquad (38)$$

$$H_{x2} = 2m_o \cos\psi \iiint dxdydz\,(x-x_o)(z-z_o)/R^5 \quad , \qquad (39)$$

$$H_{x3} = -m_o \sin\psi' \iiint dxdydz/R^3 \quad . \qquad (40)$$

Examining Eqs. (31) and (34), we see that only two integrals are required in order to calculate H_y, and from (32) and (35) we find three integrals must be evaluated in order to determine H_z.

There are a variety of ways in which to evaluate integrals such as those above. For example, one could transform to spherical coordinates and attempt to perform the integration with respect to (r,θ,ϕ). Unfortunately, this method leads to integrals that are very difficult to evaluate. On the other hand, if we use the method suggested by the geometry of Fig. 3, we can retain Cartesian coordinates and furthermore, we find that we can carry through all required integrations in closed form.

We find that integration of Eq. (38) can be done wrt x by parts with x limits being $x_c - t'/2$ and $x_c + t'/2$. This leads to

$$H_x = m_o \sin\psi' \iint dydz \{(x_o - x_c - t'/2)[(x_o - x_c - t'/2)^2 + (y_o - y)^2 + (z_o - z)^2]^{-3/2} - (x_o - x_c + t'/2) \times [(x_o - x_c + t'/2)^2 + (y_o - y)^2 + (z_o - z)^2]^{-3/2}\}$$
$$+ m_o \sin\psi' \iiint dxdydz/R^3 \quad . \qquad (41)$$

We notice that the last term of (41) exactly cancels H_{x3} as given by (40).

Assuming $t'/2$ is small compared to the other terms in each integrand, we can expand the denominators of (41). When this is done, we find terms of order t'^2, t'^4, etc. cancel exactly, and terms of order t', t'^3, etc. remain. However, in the next step of integration wrt z, terms of order t'^3, t'^5, etc. all integrate to zero. Accordingly, only terms of

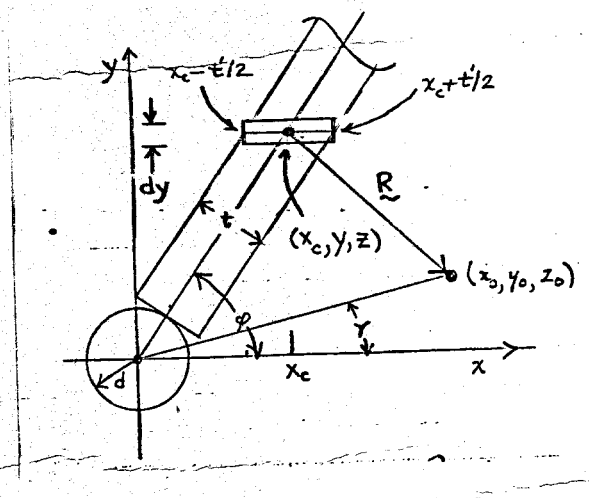

Figure 3. Geometry for integration of the contributions to the magnetic field at (x_o,y_o,z_o) due to a distribution of dipoles in the thin sheet of thickness t. Integration wrt x is over a cylinder of length t' in the x-direction with cross sectional area dydz. Here, $t' = t/\sin\phi$. The limits of integration are from $x_c - t'/2$ to $x_c + t'/2$. Thickness t is exaggerated for clarity. Actually, t is only on the order of 0.01 of the borehole radius d.

first order in t' remain. We conclude therefore that the use of the binomial expansion of the denominators is a valid step. The next step is then to perform the integration indicated by

$$H_x = m_o \sin\psi' \iint dydz \{-t'[(x_c - x_o)^2 + (y - y_o)^2 + (z - z_o)^2]^{-3/2} + 3t'(x_c - x_o)^2[(x_c - x_o)^2 + (y - y_o)^2 + (z - z_o)^2]^{-5/2}\}, \qquad (42)$$

wrt z between the limits $-\infty$ and $+\infty$. This step leads to

$$H_x = -2m_o t' \sin\psi' \int dy[(x_c - x_o)^2 + (y - y_o)^2]^{-1} + 4m_o t' \sin\psi' \int dy(x_c - x_o)^2[(x_c - x_o)^2 + (y - y_o)^2]^{-2} \qquad (43)$$

Referring now to Fig. 3, we note that $x_c = y\cos\phi/\sin\phi$. Using this in Eq. (43) leads to final integrals that can be evaluated exactly wrt y between the y limits of $+ d/\sin\phi$ and $+\infty$. Although a considerable amount of algebra is involved in reducing the results to a useful form, we give here only the final result in the two equivalent forms

$$H_x = 2m_o t' \sin\psi' \sin\phi \left[d\cos 2\phi - S\cos(\phi+\gamma)\right] / \left[d^2 - 2Sd\cos(\phi-\gamma) + S^2\right] \quad (44)$$

$$H_x = 2m_o t \sin\psi (d\cos 2\phi - x_o\cos\phi + y_o\sin\phi) / \left[d^2 - 2d(x_o\cos\phi + y_o\sin\phi) + x_o^2 + y_o^2\right]. \quad (45)$$

In (45) we have replaced $t'\sin\phi$ of (44) by the actual sheet thickness t. The form (44) is useful in calculating the signal that would be produced in a superconducting gradiometer in which two superconducting loops spaced by a distance 2S (size ?) are connected in opposition, where S is typically of the order of 0.1 d. The form (45) is useful in calculating fields at any point (x_o, y_o, z_o) either inside or away from the borehole. This latter form is derivable from the scalar magnetic potential function

$$V(x,y,z) = 2m_o t \sin\psi' \{\sin\phi \tan^{-1}\left[(d\sin 2\phi - s\sin\phi - y\cos\phi)/(d\cos 2\phi - x\cos\phi + y\sin\phi)\right] + (1/2)\cos\phi \ln\left[(d\sin 2\phi - x\sin\phi - y\cos\phi)^2 + (d\cos 2\phi - x\cos\phi + y\sin\phi)^2\right]\} - x H_o\sin\psi' - z H_o\cos\psi' \quad . \quad (46)$$

where H_o is given by Eq. (1), and $\sin\psi = H_h/H_o$ as in Eq. (3). Note that when we calculate the negative derivative of (46), we obtain not only the result (45), but the steady part $H_o\sin\psi$ of the horizontal component of the earth's field.

The field component H_y due to the sheet distrition can be calculated by the same procedure as that for H_x above. We first combine (31) and (34), integrate wrt x, expand the denominators wrt t', integrate wrt z, then integrate wrt y. Again the process involves a considerable amount of algebra. We give here only the final result in the form

$$H_y = 2 m_o t \sin\psi (d\sin 2\phi - x_o\sin\phi - y_o\cos\phi) / \left[d^2 - 2d(x_o\cos\phi + y_o\sin\phi) + x_o^2 + y_o^2\right] . \quad (47)$$

The result (47) can also be obtained directly by calculating the negative derivative wrt Y of the potential (46).

Using the same procedures as above, we can calculate the Z-component, but we find a zero contribution due to the sheet distribution. Taking the negative derivative of (46) wrt we obtain only the vertical component of the earth's field. This is what we would expect based on the earlier analysis of the formal boundary conditions.

The solutions (44) or (45) and (47) exhibit divergences similar to those of an ordinary dipole as, for example, in Eqs. (25)-(26). To see this, let the dipole moment be $\underset{\sim}{p} = \underset{\sim}{m}dxdydz$ in (25)-(26), where $\underset{\sim}{p}$ is a vector dipole of finite moment. Note then that when $R \to 0$, R^5 in the denominator $\to 0$ much faster than $R^2 \to 0$ in the numerator. Thus, at the center of the dipole, the fields seem to be infinite. This center is not available for a field measurement because it is inside the magnetic matter. In Eqs. (44) and (47), we would have the same divergence problem at the center of the sheet edge, i.e., at $S = d$, $\gamma = \phi$, or $\cos(\phi - \gamma) = 1$. In this case, $(d - S)^2$ in the denominator goes to zero faster than $(d - S)$ in the numerator does. One way to avoid this divergence difficulty is to perform the integrations over y, as indicated in Eq. (43), over the limits $y = d\sin\phi + t\cos\phi/2$ to $y = +\infty$, rather than from $y = d\sin\phi$ to $+\infty$. It turns out that the position $y = d\sin\phi + t\cos\phi/2$ is not available to us for a field measurement because it is inside the magnetic sheet.

There is no guarantee that we would have been able to avoid this same divergence difficulty even we had solved the problem by potential theory. With such an approach we would have used the magnetic boundary conditions, Eqs. (4), on the edge of the sheet at r = d, as well as on the sidewalls.

However, the existence of the divergences need not prevent our use of our distributed dipole solutions (44), (45), and (47), just as they do not prevent the widespread practice of using ordinary dipole solutions. It simply means that the region of use must be wisely chosen. For example, in our case we will consider only points such that $S/d \ll 1$, or $S/d \gg 1$ in the use of Eqs. (44)-(47). These limitations make the solutions valid for applications to superconducting gradiometers and superconducting magnetometers, as in the next section.

IV. SUPERCONDUCTING GRADIOMETER AND MAGNETOMETER ROTATION SIGNALS.

We can detect the existence of a local magnetic anomaly, such as that due to a ferrofluid-filled hydrofracture crack, by the use of a superconducting loop system capable of rotation about a vertical axis. The particular property of a superconducting loop that makes this possible is as follows: London, 1950 showed that when such a loop is inserted in a static magnetic field of magnetic induction $\underset{\sim}{B}$, a screening current I is established in the loop that just compensates the magnetic flux $\underset{\sim}{B}\cdot\underset{\sim}{A}$ that was present before the loop was inserted. This screening current I is just $\underset{\sim}{B}\cdot\underset{\sim}{A}/L$, where L is the loop inductance. If $\underset{\sim}{B}$ changes to a new value $\underset{\sim}{B}'$, I instantly changes to $I' = \underset{\sim}{B}'\cdot\underset{\sim}{A}/L$. We contrast this property with that of a normal metal loop which cannot have zero resistance. In this case, the current appears only as a transient that flows only as long as $\underset{\sim}{B}$ is changing with respect to time.

The area vector $\underset{\sim}{A}$ of a superconducting loop placed near the center of the borehole, i.e., near the z-axis and x-y plane of Fig. 2, can be expressed in the form,

$$\underset{\sim}{A} = A(\underset{\sim}{i}\sin\theta\cos\gamma + \underset{\sim}{j}\sin\theta\sin\gamma + \underset{\sim}{k}\cos\theta), \quad (48)$$

where A is the area (πa^2 for a circular loop), θ is the angle of tilt of the loop axis with respect to the z-axis, and γ is the azimuth of the loop axis in the x-y plane. When the loop axis lies exactly in the x-y plane, θ is exactly 90°. Since this ideal case is seldom achieved in practice, we let θ equal 90° - dθ. Thus, the signal current in a superconducting loop with axis nearly in the x-y plane would be,

$$I = (\mu_o A/L)\left[(H_x + H_o\sin\psi)\cos\gamma(1 - d\theta^2/2 + \ldots)\right.$$
$$\left. + H_y\sin\psi(1-d\theta^2/2+\ldots) + H_o\cos\psi\,(d\theta-\ldots)\right], \quad (49)$$

where H_x and H_y are due to the local anomaly as expressed by Eqs. (44)-(47). This is the form of the current due to a single pickup loop that would be fed via shielded superconducting leads to the SQUID sensor.

The portion of the above signal due to the magnetic sheet (or hydrofracture crack) is

$$I_m = (\mu_o A/L)(H_x\cos\gamma + H_y\sin\gamma) \quad . \quad (50)$$

Substituting (44) and (47) into (50), with S = 0, we obtain for the part in parentheses $2m_o(t/d)\sin\psi'$ x $\cos(2\phi - \gamma)$. The rotational behavior of I_m is shown in Fig. 4. It may be difficult in practice to separate this desirable signal from the undesirable portion,

$$I_u = (\mu_o A/L)\left[-(H_x\cos\gamma + H_y\sin\gamma)d\theta^2/2\right.$$
$$\left. + H_o\sin\psi\cos\gamma(1-d\theta^2/2) + H_o\cos\psi\,d\theta\right]. \quad (51)$$

The largest component of I_u, $H_o\sin\psi\cos\gamma(1 - d\theta^2/2)$, exceeds the desirable signal I_m in amplitude, while the part $H_o\cos\psi\,d\theta$ only adds a constant term, when dθ is constant. In a borehole measurement, one can expect dθ to be as large as 5° (0.087 radians). In principle, this constant term could be accounted for in data processing. However, if dθ oscillates due to wobbling of the logging tool while the loop axis is being rotated with respect to angle γ, an undesirable modulation will occur. We will see later how this essentially disappears in a two-loop gradiometer measurement.

In principle, the largest component of I_u can be subtracted away in data analysis by a number of computational techniques. The objective is to determine the phase of the signal I_m, as shown in Fig. 4, with respect to the phase of $H_o\sin\psi\cos\gamma$. One method is to cross correlate with a $\cos\gamma$ voltage of adjustable amplitude and phase. However, when the other two contributions of I_u are large, such a calculation may contain large uncertainties.

The main objection to using only one single loop system (superconducting magnetometer) is that, even after data analysis, there will still remain a 180° ambiguity in any determination of the crack azimuth. Combined gradiometer and magnetometer signals may be required to eliminate this ambiguity. Various magnetometer signals are shown in Fig. 4.

The gradiometer signal is obtained by subtracting the current in a loop at the position (x_o = S$\cos\gamma$, y_o = S$\sin\gamma$) from that in a loop at (x_o' = -S$\cos\gamma'$, y_o' = -S$\sin\gamma'$). The fields contributing to these currents are H_x, H_y and H_x', H_y', as described by Eqs. (45) and (47), respectively. The signal currents to be subtracted, are,

$$I/\mu_o = (A/L)\left[(H_x + H_o\sin\psi)\cos\gamma(1 - d\theta^2/2)\right.$$
$$\left. + H_y\sin\gamma(1 - d\theta^2/2) + H_o\cos\psi\,d\theta\right],$$
$$I'/\mu_o = (A'/L')\left[(H_x' + H_o\sin\psi)\cos\gamma'(1 - d\theta'^2/2)\right.$$
$$\left. + H_y'\sin\gamma'(1 - d\theta'^2/2) + H_o\cos\psi\,d\theta'\right], \quad (52)$$

where A'/L' can be written as (A/L) + d(A/L), γ' as γ + dγ, and dθ' = dθ + δdθ. Note that while dθ' and dθ represent small deviations from the vertical due to tilting of the whole instrument, δdθ represents an instrumental imperfection due to the fact that the vertical diameters of the two loops are not perfectly parallel. dγ = γ' - γ is also due to an instrumental imperfection in that the horizontal diameters of the loops are not parallel. For typical loop inductances on the order of 1 microHenry, A'/L' is found to have the form,

$$(A/L)\left[1 + (dR/R)(1 - u_oR/L) - 2dR^2/R^2 + \ldots\right] \quad ,$$

where R is the loop radius and dR+ R is the loop radius of L'. For typical R of 0.01 m, μ_oR/L is negligible, as is dR^2/R^2. Thus, the imperfection d(A/L) is practically equal to (A/L)(dR/R). In practice, one can produce two loops with dR/R only as small as about 10^{-4}. Similarly, dγ and δdθ can only be made to about 10^{-4} to 10^{-5}. However, effective gradiometer imbalances can be reduced to about 10^{-6} by the use of small superconducting trim tabs that can be fine positioned by screw adjustments.

Expanding the second equation of (52) and subtracting the first, we obtain the net gradiometer signal

$$(I' - I)/\mu_o = (A/L)\left[(H_x' - H_x)\cos\gamma + (H_y' - H_y)\sin\gamma\right](1 -$$
$$d\theta^2/2) + d(A/L)(H_x'\cos\gamma + H_y'\sin\gamma) + (A/L)d\gamma(H_y'\cos\gamma$$
$$- H_x'\sin\gamma) + (A/L)H_o\sin\psi\left\{\left[d(A/L)/(A/L) - d\theta\delta d\theta\right]\cos\gamma\right.$$
$$\left. - d\gamma\sin\gamma\right\} + (A/L)H_o\cos\psi\left[\delta d\theta + d(A/L)/(A/L)\right], \quad (53)$$

where terms of the order of d(A/L)dγ, dγ(dθ δdθ), etc, have been neglected. The leading term in (53) is the conventional gradiometer signal of the crack anomaly that we will discuss further below. Only the instrument axis tilt factor ($1-d\theta^2/2$) affects this signal, and for a tilt of 5°(0.087 radians) this

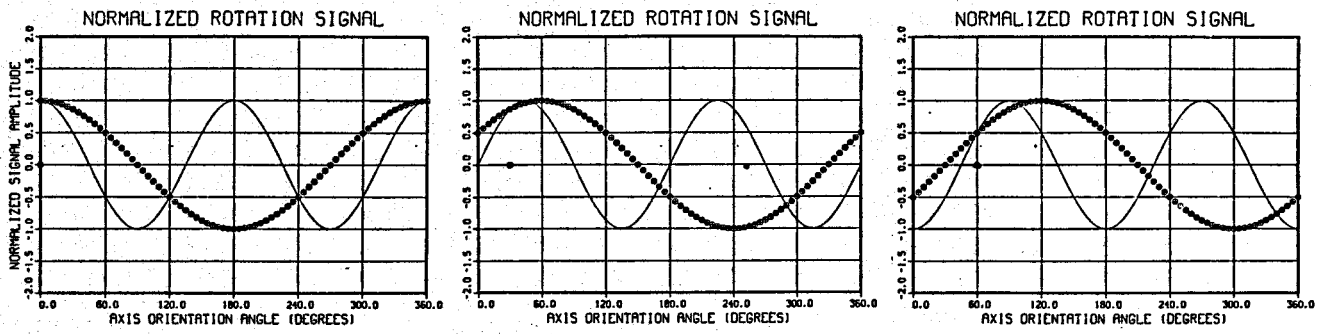

Figure 4. Curve defined by circles is the rotation signal amplitude for a single superconducting magnetometer loop with axis (loop normal) in the x-y plane as a function of the axis orientation angle γ for various crack azimuth angles ϕ. Curve shows behavior described by Eq. (50) and has normalized form $\cos(2\phi - \gamma)$. Thus, it exhibits a two-fold ambiguity with respect to azimuth ϕ. Solid curve is the rotational signal for an axial gradiometer with axis in the x-y plane, as given by the part in square brackets in Eq(57). The compact form of these square brackets is simply $\cos(3\phi - 2\gamma)$, and exhibits a three-fold ambiguity with respect to ϕ. Solid dots indicate the azimuth ϕ. Note the sensitivi- of the signal phase angle to the azimuth angle ϕ.

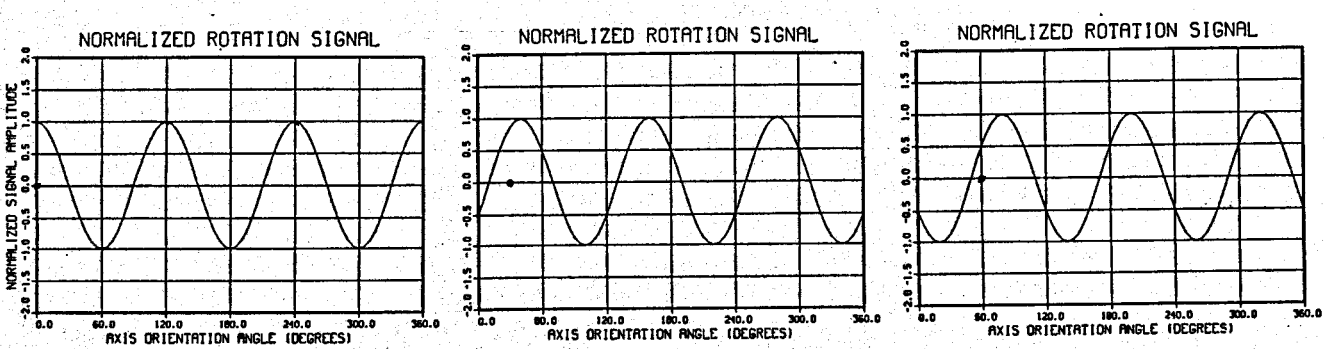

Figure 5. Rotation signal amplitude for a second-derivative axial gradiometer system versus the angle γ of rotation of the axis in the x-y plane. The azimuth ϕ f the hydrofracture crack (or sheet) is indicated by the solid dot on each graph. The signal shown is a plot of that portion of Eq. (58) in square brackets. This expression can be condensed into the more-compact form $\cos(4\phi - 3\gamma)$, which clearly shows the four-fold ambiguity of the signal.

amounts to about (1 - 0.004) but can be an annoyance if dθ is changing with respect to time due to wobble of the instrument about the vertical axis.

The desired signal in (53) has a maximum value of $(0.5\ H_o \sin\psi)(t/d)(S/d)$ which approximately equals about $5 \times 10^{-4} H_o \sin\psi$ for typical values of crack thickness = 1 mm, borehole radius d = 10 cm (4"), S/d = 0.1, and ferrofluid magnetic permeability of about 1.25. Therefore, it is required that the undesirable portions of (53), i.e., the second, third, and fourth lines, be very small compared to $0.0005\ H_o \sin\psi$. It is clear that the untrimmed balance figures of $d(A/L)/(A/L)$, $d\gamma$, and $\delta d\theta$ on the order of 10^{-4} are not satisfactory because the undesirable signals could easily amount to 0.3 to 0.5 times the desirable signal. Trimming the superconducting tabs to give balance figure of 10^{-5} is barely acceptable because the undesirable signal could still be as large as 5 % and be modulated by $\cos\gamma$. Ideally, the gradiometer balance figures should be 10^{-6} for the problem at hand. Fortunately, such a fine balance figure can be achieved by present state-of-the-art techniques that involve fine adjustments of superconducting trim tabs and loops.

While Eq. (53) describes, in its first line, the form of the gradiometer signal, the detailed properties are required in order to establish a relation between this signal and the azimuth of the magnetic sheet. These properties can be determined from Eqs. (44) or (45) and (47). In (44) we put $x_o = S\cos\gamma$, $y_o = S\sin\gamma$. Now we will let $S = S_o + s$ be the radius of the center of a superconducting pickup loop. The reason for this procedure is that it will lead to equations for both the first and the second derivative gradiometers. To see how this comes about we first reexpress Eq. (44) in the form,

$$LI/A\mu_o = (2m_o t \sin\psi')\left[(d\cos 2\phi)/D - (S_o + s)\cos(\phi + \gamma)/D\right] / \left[1 + 2sS_o/D - 2d(S_o + s)\cos(\phi - \gamma)/D\right] , \quad (54)$$

$$D = d^2 + s^2 + S_o^2 \ . \quad (55)$$

If we now let

$$s/d \quad (S_o + s)/d \quad \ll 1 \ ,$$

then, on expanding the denominator of (54), we can retain terms with factors (ts/D) and $(ts/D)(dS_o/D)$, and neglect higher order terms.

We shall carry out this expansion of (54) first with S_o held fixed at a plus value and then calculate I with $s = +s$ and calculate I' with $s = -s$. As indicated by (53), this is multiplied by $\cos\gamma$. We repeat this step with Eq. (47) and multiply this by $\sin\gamma$. The resulting signal, equivalent to (53), then takes the form

$$I' - I = (A\mu_o/L)(2m_o\sin\psi')\left\{(ts/D)\left[2\cos 2\phi - 4d^2\cos(2\phi-\gamma)\cos(\phi-\gamma)/D\right] + 4(ts/D)(dS_o/D)\left[\cos(2\phi-\gamma) - 4(d^2/D)\cos^2(\phi-\gamma)\cos(2\phi-\gamma) + 2\cos\phi\cos(\phi-\gamma)\right]\right\} \quad (56)$$

For the case of a two-coil first derivative axial gradiometer with coil spacing 2s, we set $S_o = 0$ and, with $s^2/D \ll 1$, we obtain the signal,

$$I_g = (A\mu_o/L)(4m_o\sin\psi')(ts/d^2)\left[\cos 2\phi - 2\cos(2\phi-\gamma)\cos(\phi-\gamma)\right] \ . \quad (57)$$

The portion of this signal in square brackets is plotted in Fig. 4 for various values of the azimuth angle ϕ of the magnetic sheet (or hydrofracture crack). We notice that this signal is a second harmonic of the magnetometer signal which has the form $\cos(2\phi - \gamma)$. Fig. 4 shows also that the phase of the gradiometer signal can be used to determine the azimuth angle ϕ.

We now consider the case of two sets of two coils each, all with a common axis. Let the center of the first set be at $+S_o$ and that of the second set at $-S_o$, and connect the superconducting leads from the two first-derivative gradiometers so that the signal currents are in opposition. The difference signal can be calculated directly from Eq. (56). We obtain,

$$I_2 = (u_o A/L)(16m_o\sin\psi')(ts/d^2)(S_o/d)\left[\cos(2\phi-\gamma) - 4\cos^2(\phi-\gamma)\cos(2\phi-\gamma) - 2\cos\phi\cos(\phi-\gamma)\right] \quad (58)$$

where again $s^2/D \ll 1$ and $d^2 \approx D$. The portion of this second derivative signal in square brackets is shown in Fig. 5 as a function of rotation angle, for various values of azimuth angle ϕ. We notice that this signal is a third harmonic of the magnetometer signal which varies as $\cos(2\phi - \gamma)$. Notice also that the phase varies with respect to ϕ in such a way that the signal can be used as an indicator of azimuth ϕ. However, the signal exhibits a 180° ambiguity with respect to ϕ.

It is important in acquiring experimental data to take gradiometer rotation data prior to putting ferrofluid in the thin sheet (or hydrofracture crack), for two reasons. First, if the gradiometer balance is poor, say 10^{-4} to 10^{-5}, it will be necessary to subtract a significant magnetometer contribution from the overall signal with ferrofluid. Secondly, the earth's field derivative makes a contribution and we need to know its magnitude. We have already discussed the imbalance factors. We will now calculate the horizontal component of the earth's field derivative. Consider Eq. (52) with sheet factors H_x and $H_y = 0$. From Eqs. (1)-(3) we have $H_h = H_e \sin\theta_e$. To see how θ_e changes as the center of a gradiometer loop at +s is rotated, note that the geographic colatitude will vary as $u + s\cos\gamma/a$, while the colongitude will vary as $w + s\sin\gamma/a$. Substituting these in Eq. (2) leads to

$$\sin\theta_e' = \sin\theta_e + (s/a)\tan\theta_e\{-\cos\gamma[\sin u\cos u_o + \cos u\sin u_o\cos(w-w_o)] + \sin\gamma\sin u\sin(w-w_o)\}, \quad (59)$$

(59)

Thus, the gradiometer signal component due to the derivative of the horizontal component of the earth's field will be,

$$I_e = (Au_oH_e/L)(2s/a)\tan\theta_e\{\text{term of (59) in curly brackets}\} . \quad (60)$$

When the gradiometer 1/2 spacing s is 2 cm (typical), then the factor $2 s H_e \tan\theta_e/a$ is only about 10^{-9} gauss. This is smaller than the contribution of the horizontal component of the earth's field due to gradiometer imperfection. When the balance figure is only 10^{-6}, the earth's field could contribute as much as 10^{-7} gauss to the overall gradiometer signal.

V. EXPERIMENTAL

We discuss now the experimental setup used to test the feasibility of the concepts developed in the earlier sections of this paper.

The system was prepared to our specifications by S.H.E. Corporation and had the following features:

The axial gradiometer axis was fixed at a 45° angle with respect to the vertical axis of the system and that of the fiberglass liquid helium dewar. We constructed a plywood cradle to hold the dewar and SQUID system that could be tilted to a 45° angle with respect to the vertical. This cradle was mounted on a plywood rotary table that could be rotated through 360° around the vertical axis. All parts were assembled with non magnetic screws and glues.

The reason for using such an arrangement at a magnetically quiet field test site is as follows: By rotating the dewar in its cradle to a proper position, and then tilting the cradle 45°, the gradiometer axis is brought to a vertical position. Fine adjustments of the superconducting trim tabs were then made as the rotary table was rotated through 360°. Small corrections of the axial position of the dewar in its cradle and of the tilt angle, plus final adjustments of the trim tabs then achieved the desired balance figure of about 5×10^{-6}. Three additional gradiometer tabs were preset at the factory and not later touched.

After balancing the gradiometer with its axis vertical, the dewar was rotated 180° in its cradle. With the cradle vertical axis again tilted 45°, we then position the gradiometer axis in a horizontal position, i.e., in the - planes of Figs. 1, 2, 3.

As we have discussed after Eq. (53), a balance figure of 5×10^{-6} should be satisfactory for the study of a hydrofracture crack emanating from a borehole of 10 cm (4") radius. Unfortunately, our equivalent borehole radius for the feasibility experiment was around 60 cm. This limitation was because we could not move panels closer than .

The gradiometer was constructed of two two-turn coils of fine niobium wire wound on a fused quartz form of 5.7 cm diameter with a 4.25 cm spacing between coils. Leads to the S.H.E. Corporation point-contact toroidal SQUID were shielded with superconducting braid. The pickup loop inductance was designed to match the SQUID sense coil inductance of about 2 microhenries. The system gradient sensitivity was (lower case x):

$$5.5 \times 10^{-6} \text{ (G/cm)/volt on x1 range}$$
$$5.5 \times 10^{-7} \text{ (G/cm)/volt on x10 range}$$
$$5.5 \times 10^{-8} \text{ (G/cm)/volt on x100 range,} \quad (61)$$

where the range refers to the sensitivity switch positions of the S.H.E. Corporation Model 300 SQUID data acquisition electronics system (10 volt full scale).

We simulate a hydrofracture crack filled with ferrofluid by the use of a thin sheet of ferrofluid confined by parallel lucite panels. The size of each sheet was about 2.7 m high by 1.4 m wide. A sheet thickness averaging about 1.5 mm was achieved by the use of 2-56 brass screws and brass washers as spacers. The holes for these screws were drilled to match through two panels on a face-centered square lattice array with a six-inch spacing. The screw-washer-nut assembly was made leak tight by sealing with Duco cement. Precautions were taken to use only nonmagnetic materials in the construction of these panels. Although 12 panels were made in order to simulate a hydrofracture crack of some 30 m extent, only three were needed in the actual experiment. Adding a fourth panel on the ϕ azimuth made only an insignificant difference in the gradiometer rotation signal.

The magnetite ferrofluid needed to fill the thin sheet panels was manufactured in our laboratory by a process described in a patent for ferrofluid mass production (Reimers, et al, 1974). We used two parts of ferric chloride to one part of ferrous chloride in water solution. When reduced by ammonium hydroxide, the process precipitates colloidal sized magnetite particles. After washing and decanting off the solution, high-quality kerosene (Jet A fuel) is added and the particles can be stirred into temporary suspension. Peptizing with oleic acid then coats and separates the particles so that the magnetic forces tending to agglomerate the particles can be overcome by Brownian motion.

We produced some 140 liters for our experimental use at a cost of about $7,000. In small quantities, a liter of ferrofluid with a magnetic permeability of about 2.0 costs about $800 on the commercial market.

We measured the magnetic permeability of each batch during manufacture and found batches with k_m varying from 1.15 to 1.7. The value obtained for the ferrofluid used in the experiments was about 1.25.

The experimental technique involved taking SQUID data at 10° angles of the rotary table with respect to magnetic north with the magnetic panels removed far enough away so as not to affect the signal. The runs were then repeated with the panels in position at a desired angle ϕ. Twenty four ϕ values were chosen starting at $\phi = 0$ for magnetic north. The S.H.E. model 30 output signal was fed to a digital voltmeter for easy readout and the data were recorded to 3 1/2 decimal digits. We used ac power from a motor generator set only for tuning up the equipment. During data taking, we used only battery power. The nearest power line that could give 60 Hz interference was 1.2 miles away.

VI. DATA ANALYSIS

Because our gradiometer balance figure was not better than 5×10^{-6}, it was necessary to take data both before and after the panels were positioned at desired ϕ angles. The desired signal was obtained by subtracting the before from the after signal. Some of the results are shown by the experimental points plotted in Fig. 6. This procedure gives the gradiometer component essentially free from the undesirable magnetometer component.

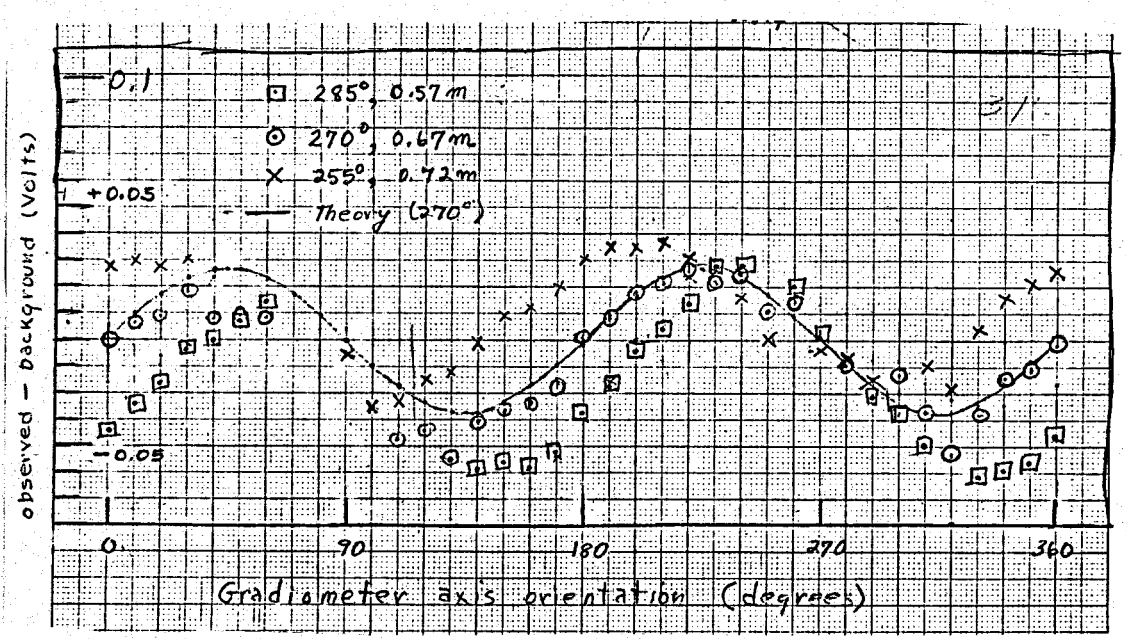

Figure 6. Gradiometer rotation signal data for a sheet magnetic anomaly at different sheet azimuths (ϕ values). The ordinate is the observed (after) signal minus the background (before) signal using the xl range of the SQUID instrumentation. Referring to (61), we note that the 0.01 V ordinate increment corresponds to 5.5×10^{-8} G/cm. The abcissa is the rotation angle γ. The solid curve shows the theory for the axial first-derivative gradiometer, as given by Eq. (57), for $\phi = 270°$. The amplitude of the theoretical signal is adjusted to give the best least-squares fit to the 270° experimental data (solid circles). Standard deviations of the fits to these data are given in Table 2.

The goal of this work is to determine the azimuth ϕ of the magnetic sheet (or hydrofracture crack) with an uncertainty of not greater than $\pm$ 15°. In addition to this local accuracy requirement, it is necessary to resolve the ambiguities: 180° for the magnetometer (label m); 120° for the gradiometer (label g); and 90° for the second-derivative gradiometer (label 2).

We consider first the question of local accuracy. Let us assume that we have obtained the signal in desired form, either by subtracting the background signal, as we did for the data of Fig. 6, or else, by a digital filtration technique. We can record these signals in either analog or digital form in preparing the data for subsequent computer analysis. The amplitudes of the SQUID output signals may range from 0 to 10 volts.

We denote the possible experimental signals by $v_m(\gamma_i)$, $v_g(\gamma_i)$, and $v_2(\gamma_i)$, where i is the index for the rotation angle γ_i as well as for the signals. It is convenient to hold the incremental angle $\Delta\gamma$ always at a constant value. For the data of Fig. 6, we let i = 1, 2,...,N, with N = 36, i.e., $\Delta\gamma$ = 10°.

When we express the corresponding theoretical signal in the forms $w_m(\gamma_i, \phi_j)$, $w_g(\gamma_i, \phi_j)$, and $w_2(\gamma_i, \phi_j)$, respectively, the formal integral expression for the coefficient of cross correlation can be written in terms of the sums,

$$R_{vw}(\phi_j) = \sum_i v(\gamma_i)\, w(\gamma_i, \phi_j) \Big/ \left[\sum_i v^2(\gamma_i) \sum_i w^2(\gamma_i, \phi_j) \right]^{1/2}, \quad (62)$$

in which the subscripts for v, and w have been omitted. We found earlier that $w(\gamma_i, \phi_j)$ can be expressed in the form $f(\phi_j) \cos(p\,\phi_j - q\gamma_i)$, where p and q are integers. We identify p = 2, q = 1 with label m, p = p = 3, q = 2 with label g, and p = 4, q = 3 with bel 2.

In evaluating R_{vw}, we calculate values of $w(\gamma_i, \phi_j)$ for the same set of γ_i values used to obtain the experimental data, i.e., the set of $v_g(\gamma_i)$ shown in Fig. 6. For a few values of γ_i, we were unable to obtain a signal because of experimental reasons. These points are indicated by the gaps on Fig. 6. Thus, for every v_i obtained, we use only the corresponding calculated w_i. The R_{vw} values calculated

TABLE 2.

Coefficient of cross correlation between the experimental gradiometer signal $v(\gamma_i)$ of Fig. 2 and the function $f(\phi_j)\cos(3\,\phi_j - 2\,\gamma_i)$ as calculated via Eq. (62). The top number for each angle ϕ_j is the coefficient $R_{vw}(\phi_j)$. The numbers in parentheses are the standard deviations, in volts, of the fitting functions, as calculated via Eqs. (65) and (67). The numbers in square brackets are the estimated standard errors of the azimuth ϕ determinations.

Experimental ϕ / ϕ_j:	240°	255°	270°	285°	300°
255°	0.703 (0.0160) [11.9°]	0.846 (0.0118) [7.9°]	0.560 (0.0220) [22.3°]		
270°		0.709 (0.0161) [12.2°]	0.911 (0.0094) [5.7°]	0.645 (0.0174) [14.4°]	
285°			0.712 (0.0241) [12.6°]	0.851 (0.0180) [7.7°]	0.524 (0.0292) [19.1°]

via Eq. (62) are shown in Table 2.

The quality of the fit of a theoretical function $w(\gamma_i, \phi_j)$ for a chosen ϕ_j to an experimental set of data $v(\gamma_i)$ can be determined by calculating the standard deviation. Since a residual is of the form,

$$r_i(\phi_j) = v(\gamma_i) - w(\gamma_i, \phi_j) \quad ,$$

we obtain for the sum of squares of residuals,

$$\sum_i r_i^2(\phi_j) = f^2(\phi_j) \sum_i \cos^2(p\,\phi_j - q\,\gamma_i) - f(\phi_j) \sum_i v(\gamma_i) \cos(p\,\phi_j - q\,\gamma_i) + \sum_i v^2(\gamma_i) \qquad (63)$$

Minimizing the left side of (63) with respect to f leads to,

$$f(\phi_j) = \sum_i v(\gamma_i) \cos(p\,\phi_j - q\,\gamma_i) \Big/ \sum_i \cos^2(p\,\phi_j - q\,\gamma_i) \quad . \qquad (64)$$

This calculation then leads to $w(\phi_j,\gamma) = f(\phi_j) \times \cos(p\,\phi_j - q\,\gamma)$ that best fits the set of experimental data $v(\gamma)$. The standard deviation of this fit is therefore

$$\sigma_w(\phi_j) = \left[\sum_i r_i^2(\phi_j)/(N-1) \right]^{1/2} \quad . \qquad (65)$$

Using this formula, we obtain the results shown in in the parentheses in Table 2.

Table 2 exhibits two interesting facts, e.g., when the angle ϕ_j chosen to characterize the theoretical function is the same as the azimuth ϕ identified with the experimental rotation signal, then the cross correlation coefficient $R_{vw}(\phi_j)$ is a maximum and, at the same time, the standard deviation of the fit, $\sigma_w(\phi_j)$, is a minimum.

Consequently, in an actual field application in which the magnetic sheet azimuth ϕ is unknown, we would repeat the correlation and least squares fitting calculations (by computer of course) until we found the ϕ_j parameter giving the largest R_{vw}, and simultaneously, the smallest σ_w. Thus, we could assert that this ϕ_j parameter was close to the true azimuth ϕ of the sheet (except for the ambiguity to be discussed later). The error of this process can be expressed in terms of the standard error σ_ϕ such that the azimuth determined would have the form,

$$\phi = \phi_j \pm \sigma_\phi \quad . \qquad (66)$$

In order to estimate σ_ϕ, we will utilize the σ_w of Table 2 and the value of $f(\phi_j)$ found in the calculations via Eq. (64), and resort to the principles of propagation of errors. Here, if we have a function of two variables, such as $w(\phi_j, \gamma)$, the errors obey the relation,

$$\sigma_w^2(\phi_j) = (\partial w/\partial \phi_j)^2 \sigma_\phi^2 + (\partial w/\partial \gamma)\, \sigma_\gamma^2 + 2(\partial w/\partial \phi_j)(\partial w/\partial \gamma)\, \sigma_\phi \sigma_\gamma \quad . \qquad (67)$$

It is reasonable to assume $\sigma_\gamma = 0$ since the measurement error of γ is probably less than 0.02 radians. Then, since w is periodic in γ, the relation (67) can be expressed in the form

$$\sigma_\phi^2 = \sigma_w^2 \Big/ \overline{(\partial w/\partial \phi_j)^2} \quad . \qquad (68)$$

Thus, for the possible forms of w, we

$$\overline{(\partial w/\partial \phi_j)^2} = (\partial f/\partial \phi_j)\, \overline{\cos^2(p\,\phi_j - q\,\gamma)} - 4f(\partial f/\partial \phi_j)\, \overline{\cos(p\,\phi_j - q\,\gamma) \sin(p\,\phi_j - q\,\gamma)} + 4\,f^2\, \overline{\sin^2(p\,\phi_j - q\,\gamma)} \quad . \qquad (69)$$

The average of the middle term of (69) is zero while that of the first and last terms is π. Thus, we obtain as a first estimate of the error

$$\sigma_\phi = \sigma_w \pi^{-1/2} \left[4 f^2 + (\partial f / \partial \phi_j)^2 \right]^{-1/2},$$

in which the units of σ_ϕ are radians and those of σ_w and f are volts. We find that f depends on the average square of the experimental signal amplitude but very little on the value of ϕ_j chosen for the fitting function. Accordingly, we shall assume that $(\partial f / \partial \phi_j)$ is negligible compared to 4 f. This leads to

$$\sigma_\phi \approx \sigma_w / (2 \pi^{1/2} f) . \qquad (70)$$

Estimates of σ_ϕ based on Eq. (70) are shown in Table 2 (in degrees rather than in radians).

These final results of Table 2 indicate that when when R_{vw} is a maximum and, at the same time, σ_w is a minimum, the error of azimuth determination is only about one half the requirement of $\pm$ 15° mentioned earlier, except for possible ambiguities.

Ambiguities occur because a particular measuring system obtains the same signal function $w(\phi,\gamma)$ for more than one value of the sheet (or crack) azimuth ϕ. Since the magnetometer, gradiometer, and second-derivative gradiometer are all described by the same type of signal function,

$$w(\phi,\gamma) = f(\phi) \cos(p\,\phi - q\,\gamma) ,$$

the ambiguities are different simply because the integer sets (p,q) are different for each type of instrument.

We can characterize the ambiguities by finding the angles γs at which each signal has maximum amplitude. The possible ambiguities are then evident by reference to Table 3. The reason for this particular choice of characterization is that, in data processing, the maxima of signals are easier to discern than the minima or the zeroes. The signals referred to in Table 3 are the functions $w(\phi,\gamma)$ which, we presume, will have been determined by least-squares adjustments with respect to observed signals $v(\gamma)$s.

In order to account for ambiguities in field applications in which the azimuth of the crack is unknown, it will be necessary to do two types of measurements at the same time. For example, we could have a logging tool with both a magnetometer loop (with its SQUID) and a first-derivative gradiometer (with its separate SQUID). A similar system is shown in Fig. 3 in the paper by Steyert and Overton (1980, these proceedings). In this example, an axial and a planar gradiometer are indicated.

To see how such a dual system eliminates the ambiguity, refer to Table 3. Consider a gradiometer signal which peaks at γ = 45° and 225° when azimuth ϕ = 30°, 150°, and 270°. A magnetometer with its axis parallel to that of the gradiometer would have its maxima at γ = 60° when ϕ = 30° and 210°. We would thus determine that ϕ = 30° since this is the only ϕ value satisfying simultaneously both sets of rotation data.

Examination of Table 3 shows that a system with a magnetometer and a second-derivative gradiometer would not have the capability of eliminating ambiguities. On the other hand, a system with a first-derivative gradiometer and a second-derivative gradiometer can resolve the ambiguity and, at the same time, provide freedom from the undesirable signal components that appear in the magnetometer signal.

TABLE 3.

Rotation angles γs at which maxima of signal functions occur versus sheet (crack) angle ϕ. w_m, w_g, and w_2 denote magnetometer, first-, and second-derivative gradiometers, respectively. All angles are in degrees.

ϕ	γ at w_m(max)	γ at w_g(max)	γ at w_2(max)
0	0	0, 180	0, 120, 240
30	60	45, 225	40, 160, 280
60	120	90, 270	80, 200, 320
90	180	135, 315	120, 240, 360(0)
120	240	0, 180	40, 160, 280
150	300	45, 225	80, 200, 320
180	0	90, 270	120, 240, 360(0)
210	60	135, 315	40, 160, 280
240	120	0, 180	80, 200, 320
270	180	45, 225	120, 240, 360(0)
300	240	90, 270	40, 160, 280
330	300	135, 315	80, 200, 320

VI. SUMMARY AND DISCUSSION.

We have given in Section II an analysis of the polarization of a thin vertical sheet of magnetic material by the ambient earth's field. This sheet is supposed to represent a hydrofracture crack emanating radially outward in one direction from a deep borehole, this direction being specified by an arbitrary azimuth angle ϕ. We found it necessary to go into considerable detail in this analysis in order to prove that the direction of magnetization of the material inside the sheet would be parallel to the earth's field at a distance from the sheet. In earlier work (Overton, 1976) it was simply assumed, without proof, that these directions would be parallel.

After this necessary first step, we could then calculate the fields at an arbitrary point outside the sheet due to the elements of the sheet. We postulated in Section II that each volume element would exhibit a dipole moment $m\,dx\,dy\,dz$ proportional to the magnetic permeability $\mu_o k_{in}$ u_o (or magnetic susceptibility $k_{in}-1$) with direction parallel to that of the original earth's field. In order to perform the integrations over all of the dipole emements of the sheet, we had to assume that there were no mutual interactions among the elements themselves. The methods of performing these integrations are outlined in Section III, but the details were too lengthy to include there. The most important final results are expressed by Eqs. (45) and (47). The form of these results differs somewhat from those reported earlier (Overton, 1976) because, in that work, a thin wedge of magnetic material was assumed rather than the magnetic sheet considered here. The sheet is, of course, a more realistic representation of the vertical crack produced by hydrofracture.

Using the expressions for H_x in Eq. (45), and H_y in Eq. (47) and $H_z = H_z(\text{infinity})$, we could calculate in Section IV the steady state current that would occur in a circular superconducting pickup loop when that loop was inserted in the field. Of course, systems of such loops form the magnetometer, the first-derivative gradiometer, and the second derivative gradiometer. When the axes of such loops are in the horizontal plane while the systems are rotated about the vertical axis, signal currents develop that characterize the local magnetic anomaly caused by the vertical sheet. In the case of the axial gradiometers, one can determine the forms of the signal currents by replacing (x_o, y_o) by $(S\cos\gamma, S\sin\gamma)$ in Eqs. (45) and (47). Then, differentiating with respect to S leads to expressions for the signals received by these gradiometers. However, we use this procedure only as a check. We chose instead, to carry out the expansions of the expressions in terms of the ratio S/d, where S is the gradiometer loop spacing. The reason for this more-elementary procedure is that the expansion methods bring forth the interference contributions discussed at length in Section IV.

The methods used in Section IV can be extended to the derivation of the signals that would be detected by the various types of planar gradiometers. Such signals will exhibit a different type of rotation signature than those of the axial gradiometers we discuss here. However, due to space limitations, we cannot develop these equations here.

We discuss in Section V the details of the field experiments in which we used an axial first-derivative gradiometer-SQUID system. In the comparison in Section VI of the experimental data and the theoretical results summarized in Section IV, we find good agreement for the east and west quadrants but only fair agreement for the north and south quadrants. The reason for this is that, due to gradiometer imbalance being not better than about 5×10^{-6}, the magnetometer component dominated the overall signal for sheet azimuths in the north-south quadrants. We pointed out in Section VI that the nearest edge distance d of the magnetic sheet always exceeded 0.5 m whereas, in an actual borehole logging situation, d would be between 0.1 m and 0.2 m. Accordingly, in a logging situation, the anomaly part of the signal would be significantly larger, the signal-to-noise ratio greater, and the signal definition better. Thus, our field experiments have given a severe test of the theory.

We outline also in Section VI the methods of data processing that would be used in actual logging situations. The equations we use in Section VI for cross-correlation, least squares fitting, and azimuth ϕ error determination could be made a part of the software of a low-cost microprocessor that could be used in the field. It is feasible that a digital filtration processor could be used also in the field. This should make possible the separation of the interfering magnetometer and gradiometer components of the overall signal without having to resort to the before-and-after subtraction process we used in our data analysis.

Although the concept of rotating a SQUID magnetometer or gradiometer in order to obtain a signal that actually characterizes a local magnetic anomaly was first given about four years ago (Overton, 1976), the correct description of the sheet anomaly properties is given here for the first time. This work also gives the first experimental verification of the nature of these rotation signatures, as well as the mathematical bases for processing the SQUID data. In other words, the feasibility of the concepts were not actually demonstrated until we completed this present work.

The concepts discussed above would be useless if it were not possible to provide the necessary low temperature environment for the SQUID and its associated superconducting circuits. This problem has been addressed in these proceedings in a paper (Steyert, et al, 1980) which proves the feasibility of a logging tool system that houses a cryogenic environment. The system does not require the venting of cold helium gas and can be used for logging deep boreholes.

We make now the following final points. The above-discussed techniques are not limited to the study of local anomalies due to hydrofracture cracks filled with ferrofluid. Anomalies due to natural distributions of ferrous rocks or diamagnetic rocks can be studied also, whether thay be small-sized localized distributions or large sized. In these cases, rotating SQUID-magnetometers or gradiometers would be used at one location at a time. By repeating such rotation studies at an appropriate number of stations, and then using mathematical techniques similar to those described in Section VI, we could determine the properties of the distributions such as size, shape, and location.

REFERENCES

Albright, J. N. and Newton, C. A., 1980, The Characterization of Hot Dry Rock Geothermal Energy Extraction Systems--A Challenge for Science and Technology, preceding paper, these Proceedings.

Clarke, John, 1973, Low-Frequency Applications of Superconducting Quantum Interference Devices, Proceedings of IEEE, January, 1973, pp. 8-20.

Clarke, J., Goubau, W. M., and Ketchen, M. B., 1976, Tunnel Junction dc SQUID: Fabrication, Operation, and Performance, Journal of Low Temperature Physics, Vol. 25, pp. 99-144.

Giffard, R. P., Webb, R. A., and Wheatley, J. C., 1972, Principles and Methods of Low-Frequency Electric and Magnetic Measurements Using an rf-Biased Point-Contact Superconducting Device, Journal of Low Temperature Physics, Vol. 6, pp. 533-610.

Long, A., Clark, T. D., Prance, R. J., and Richards, M. G., 1980, High-performance UHF SQUID Magnetometer, Review of Scientific Instruments, Vol. 50, pp. 1376-1381.

Overton, W. C., Jr., 1976, Feasibility of Detecting Artificial Magnetic Anomalies in Hydrofractured Rock by Superconducting Gradiometer-SQUID Systems, Los Alamos Scientific Laboratory Report No. LA-6626-MS.

Reimers, G. W. and Khalafalla, S. E., 1974, Production of Magnetic Fluids by Peptization Techniques, U. S. Patent 3,843,540, Oct. 22, 1974 (domestic rights assigned to the Department of the Interior)

Seguira, M. and Heppner, J. P., 1972, The Earth's Magnetic Field, American Institute of Physics Handbook, D. E. Gray, Coordinating Editor, McGraw Hill Book Company, New York, pp. 5-264 to 5-273.

Steyert, W. A., and Overton, W. C., Jr., 1980, SQUID System Cryogenic Environment for Deep Borehole Logging, these Proceedings.

Tester, J. and Spence, R. W., 1980, private communications.